Supporting Information

de Villers-Sidani et al. 10.1073/pnas.1007885107

SI Text

Sound Intensity Thresholds in the Aged A1 and After Training. Compared with the Y group, sound intensity thresholds in the A group were increased by approximately 11 dB sound pressure level (SPL) for low (3.5 kHz) CF neurons and by approximately 5 dB SPL for high (28 kHz) CF neurons ($P < 0.001$ and $P < 0.01$, respectively; Fig. S2). No significant difference was found in the midfrequency (10–15 kHz) range ($P > 0.2$). Although oddball training had no significant impact on low frequency thresholds, we observed a small but statistically significant reduction of approximately 4 dB SPL in threshold toward Y levels in AT for high (28 kHz) CF neurons ($P < 0.05$). Total A1 sizes did not differ among the four groups ($P > 0.2$).

Effect of Age and Training on A1 Temporal Coding Reliability. We examined the reliability of temporal coding in A1 neurons in the four experimental groups using a variant of the van Rossum spike train metric (1) (*SI Methods*). This method takes into account spike numbers as well as their precise timing to provide a measure of the difference between two spike trains. This measure of difference can then be used to quantify the ease with which an ideal observer would discriminate between the occurrences of different stimuli (here, noise burst trains presented at different rates), simply by looking at the response patterns of individual A1 neurons. We calculated misclassification rates for every possible combination of noise burst stimuli used and then constructed confusion matrices for all groups (Fig. 3*E*). Compared with Y controls, misclassification rates in the A group were higher for both identical and different stimuli. Differences between the two groups were especially marked when dissimilar high-rate stimuli were presented. For example, for 13.6 vs. 17.4 pps, the misclassification rate in the Y group was 66.0% compared with 78.9% in the A group ($P < 0.0001$). Misclassification of identical stimuli as different was also more frequent in the A group, especially for slow stimulus speeds. For example, at 4.1 pps, the same rate was misclassified 28.3% of the time in the Y group compared with 37.6% in the A group ($P < 0.001$). Similar low (<20%) misclassification rates were found in both groups for stimulus rates at or below 6.6 pps. Oddball discrimination training greatly reduced misclassification rates in both aged and young groups as indexed by the spike train metric used. In AT, the probability of misclassification for combinations of dissimilar high pulse rates (10.7–17.4 pps) was not statistically different from Y levels ($P > 0.2$; Fig. 3*E*). The same was true for the confusability of similar low pulse rates (2.5–6.6 pps), which was also significantly reduced in AT compared with the A group ($P =$ 0.02–0.001). More reliable rate coding was also seen in the YT group for rates greater than 10.7 pps ($P =$ 0.01–0.0001).

Spectrotemporal Interactions in A1. The impact of training on cortical inhibition in young and aged rats was examined further by constructing the STRF of several single neurons in A1. The STRFs were obtained with spike-triggered averaging (reverse correlation) and using a "random chord" stimulus containing a spectrally and temporally dense sequence of random tone pips (2) (*SI Methods*). Representative STRFs obtained in each group are shown in Fig. S3. To compute the average inhibitory strength across the each neuron populations, the activation peaks of the STRFs were aligned and response intensity was normalized according to the total strength of activation. Then, only the inhibitory portion of the STRF was kept for the analysis. Note that the total activation intensity was not significantly different between groups. Total STRF inhibitory strength was, on average, 30% less in the naive A group compared with the naive Y group (Fig. S3; $P < 0.01$). Furthermore, tone combinations producing peak inhibition were closer in time relative to spike occurrence in the A group (Y vs. A peak delay, 55 ± 4 vs. 33 ± 9 ms; $P < 0.05$). No difference was found in the frequency position of the inhibitory peaks relative to activation peaks in any of the groups. Oddball training resulted in a significant increase in total inhibition in both trained groups compared with age-matched controls. In YT, total inhibition was increased by more than 40% ($P < 0.001$) whereas it increased by 55% in AT rats ($P < 0.001$, *t* test), whose values were equivalent to young controls ($P > 0.2$). Furthermore, in the AT group, the average inhibitory peak delays matched those found in young groups (AT average inhibitory peak delay, 54 ± 7 ms; $P < 0.05$ vs. A).

Age-Related Changes in MBP Expression. A progressive decline in subcortical myelin occurs with healthy aging in humans (3). This change is thought to contribute to age-related cognitive impairments (4). Cortical myelin density was determined in all experimental groups by semiquantitatively measuring the density of MBP expression in A1 (*SI Methods*). MBP is a homogeneously distributed major constituent of myelin (5). Compared with the Y group, a reduction of MBP immunoreactive density was noted in the A group (Fig. S6). More specifically, an approximate 35% decrease in MBP density in superficial layer I was observed in the A group compared with the Y group ($P < 0.05$). Similarly, a 38% decrease in MBP density was also noted in layers II and III ($P < 0.05$). Oligodendrocytes (Olg) were also reduced in numbers in layers I–III of A animals compared with Y (A vs. Y, 5.44 ± 1.9 cells/mm^2 vs. 1.7 ± 1.2; $P < 0.001$). Interestingly, oddball discrimination training resulted in a relative normalization of MBP levels in the AT group in layers II/III (AT, 3.9 ± 1.6% cells/mm^2; $P < 0.05$) but not in layer I ($P > 0.2$). A recovery of Olg immunoreactive cell density was also seen in the AT group (3.88 ± 1.8 cells/mm^2; $P < 0.05$).

SI Discussion

Both thalamocortical synapses and intracortical inhibitory circuit are responsible for temporal tuning in the cortex (6, 7). In our study, changes in cortical inhibition are more likely to be at play as changes in response latencies, which usually accompany lower thalamocortical transmission potency (6), were not observed. A decrease in the number of asynchronous responses in the AT rats also supports this hypothesis. Inhibitory spectrotemporal interactions were restored in the aged A1 by training. The broad increase in STRF inhibitory depth and area in the trained groups is a further indication that training resulted in greater A1 neurons stimulus specificity. Inhibitory areas observed in STRFs have been speculated to result from greater excitatory than inhibitory synapse depression and are linked to probe stimulus density (8). The precise location in the auditory axis of the change in excitatory/inhibitory balance we observed will be difficult to pinpoint until recordings in subcortical nuclei are performed. The exact mechanism by which oddball training might restore inhibition in the aging cortex remains unclear. Many of the changes observed with training could involve PV+ cells, which have intrinsic functional and structural properties that make them likely to participate in the reshaping of RFs (9, 10). They are also particularly sensitive to stimulus contrast (11), a key parameter in our training paradigm.

Environmental factors could have played a role in the emergence of A1 age-related deficits seen in this study. The auditory environment in which naive rats were kept until the time of mapping was not as rich and intellectually challenging as a natural habitat. This raises the possibility that, in humans like in rats, a chronically re-

duced level of meaningful challenging intellectual activity might be a significant etiological factor in age-related cognitive decline. In fact, the widespread improvements we observed in aged rats after auditory oddball training—a controlled form of intensive sensory enrichment—is a clear indicator that rewarding intellectual activity can have strong up-regulating effects on cortical function.

SI Methods

Mapping the Auditory Cortex. For A1 mapping, the rats were premedicated with atropine sulfate (0.02 mg/kg) to minimize bronchial secretions and with dexamethasone (0.2 mg/kg) to minimize brain edema. They were then anesthetized with pentobarbital (55 mg/kg i.p.). Supplemental doses of dilute pentobarbital were given as required to maintain the rat in an areflexic state while preserving a physiological breathing rate. The cisterna magnum was drained of cerebrospinal fluid to minimize cerebral edema. The skull was secured in a head holder leaving the ears unobstructed. The right temporalis muscle was reflected, auditory cortex was exposed, and the dura was resected. The cortex was maintained under a thin layer of silicone oil to prevent desiccation. Recording sites were marked on a digital image of the cortical surface.

Cortical responses were recorded with tungsten microelectrodes (1–2 MΩ; FHC). Recording sites were chosen to sample evenly from the auditory cortex at interelectrode distances of 125 to 175 μm. At every recording site, the microelectrode was lowered orthogonally into the cortex to a depth of 470 to 600 μm (layers 4/5), where vigorous stimulus-driven responses were obtained. The neural signal was amplified (10,000×), filtered (0.3–3 kHz), and monitored online. Acoustic stimuli were generated by using System III (Tucker-Davis) and delivered to the left ear through a calibrated earphone (STAX54) with a sound tube positioned inside the external auditory meatus. A software package (SigGen and Brainware; Tucker-Davis) was used to generate acoustic stimuli, monitor cortical response properties online, and store data for offline analysis. The evoked spikes of a single neuron or a small cluster of neurons were collected at each site.

Frequency–intensity RFs were reconstructed by presenting pure tones of 50 frequencies (1–30 kHz; 0.1-octave increments; 25 ms duration; 5 ms ramps) at eight sound intensities (0–70 dB SPL in 10-dB increments) to the contralateral ear at a rate of tone stimulus per second. RRTFs were obtained by presenting trains of broadband noise bursts (25 ms duration; 5-ms ramps) at 70 dB SPL and at various rates (2.5–17.4 pulses per second).

One to five 1-min-long trains of tone pips with of 25-ms-duration pips were presented at 1, 3, and 5 pulses per second at a sound intensity of 70 dB SPL. Each train had a frequently occurring frequency (standard) with a probability of occurrence of 90% and a pseudorandomly distributed oddball frequency presented 10% of the time with no repetition. The two frequencies in the train had constant separation of 1 octave and were chosen so they would be contained within the RF of the recorded neuron and elicit strong reliable spiking responses.

The stimulus used to obtain STRFs was created in a similar fashion than previously published (12) by adding independent tone pip trains at each one-sixth octave frequency band between 1.5 and 22 kHz. Tone pips in each independent train were 50 ms long with 5-ms on-and-off ramps and occurred following a Poisson distribution with an average of 1 pip per second. The spectrotemporal density stimulus was presented continuously for 15 min.

Behavior. The rats' behavior was shaped in three phases. During phase A, rats were trained to make a nose poke response to obtain a food reward. During phase B, rats were trained to make a nose poke only after presentation of an auditory stimulus (single 12-kHz tone pip at 60 dB SPL). During phase C, the actual training program, rats were trained at level 1 to make a nose poke only for the target stimulus (containing an oddball frequency) and not for a foil stimulus with six identical tones of frequency identical to the standard frequency (9 kHz). The tones were presented at a 60 dB SPL. Every training session started at level 1. The level was increased after three consecutive correct target identifications and decreased after a response to a nontarget (i.e., false-positive) or miss (three-up/one-down). The task difficulty was progressively increased by reducing in exponential steps the frequency difference between standards and oddballs from 0.5 octaves (level 1) to 0.02 octaves (level 6).

Training was performed in an acoustically transparent operant training chamber (20 × 20 × 18 cm, length × width × height) contained within a sound-attenuated chamber. Psychometric functions and stimulus target recognition thresholds were calculated for each training session by plotting the percentage of go responses as a function of the total number of target stimuli (i.e., hit ratio) and the percentage of false positives as a function of the total number of foils (i.e., false-positive ratio). Learning curves were reconstructed by plotting maximal level reached over successive days of training.

A single behavioral trial was defined as the length of time between the onsets of two successive tone trains. The intertrial interval was selected at random from a range of 3 to 9 s. A rat's behavioral state at any point in time was classified as either "go" or "no-go." Rats were in the "go" state when the photobeam was interrupted. All other states were considered "no-go." For a given trial, the rat could elicit one of five reinforcement states. The first four states are given by the combinations of responses (go or no-go) and stimulus properties (target or nontarget). Go responses within 3 s of a target were scored as a hit; a failure to respond within this time window was scored as a miss. A go response within 3 s of a nontarget stimulus was scored as a false positive. The absence of a response was scored as a withhold. A hit triggered the delivery of a food pellet. A miss or false positive initiated a 5 s "time-out" period during which time the house lights were turned off and no stimuli were presented. A withhold did not produce a reward or a time out.

Immunohistochemistry. At the end of recording sessions, electrolytic lesions were made at the previously functionally defined A1 borders. All rats were then received a high dose of pentobarbital (85mg/kg i.p.) and perfused intracardially with saline solution followed by 3.5% paraformaldehyde in 0.1 M PBS solution, pH 7.2. Brains were removed and placed in the same fixative containing 20% sucrose for 12 to 24 h. Fixed material was cut in the coronal or axial plane along the tonotopic axis of A1, on a freezing microtome at 40 to 80 μm. The density of PV+ cells in A1 was quantified using standard immunostaining techniques by counting all of the PV+ cells present within three 300-mm-wide A1 sections per hemisphere. Tissue was incubated overnight at 4 °C in monoclonal or polyclonal antisera (dilution 1:2,000; Sigma; for anti-PV, P3088; dilution, 1:2,000; Chemicon International; for anti-MBP, MAB1580). After exposing to biotinylated antimouse or rabbit IgG (1:100; ABC kit; Vector), samples were rinsed and treated further with streptavidin-conjugated Cy3 (red; 1:200; Jackson ImmunoResearch). Tissue from Y and A rats were always processed together in pairs during immunostaining procedures to limit variables relate to antibody penetration, incubation time, and postsectioning age/condition of tissue (13). A similar approach was also conducted for A and AT rat brain tissues. A Nikon E800 epifluorescent microscope was used to assess fluorescence in the immunostained material. An imaging system equipped with a Photometrics Coolsnap ES CCD camera (Roper Scientific) and Metamorph imaging software (Molecular Devices) was used to quantify data. PV+ cell density was evaluated in three 300-μm-wide A1 sectors (rostral, middle, and caudal) per hemisphere expending from layer 1 to the underlying white matter. Images were acquired from nonrecorded hemispheres/case, keeping exposure time constant for each series of tissue. From these images, the total numbers of PV+ cells in each cortical section was calculated and averaged. PV+ cells were classified visually as normally or weakly staining according to their fluorescence pattern, which followed a clear bimodal distribution. Typical PV+ cells showed very strong fluorescence. A group of

"weakly staining" PV+ displayed similar fluorescence intensity levels above background but at least one order of magnitude below typical PV+ neurons.

To semiquantitatively analyze alterations in MBP density that were attributable to aging or training, digital photomicrographs of A1 cortical sections were taken with a 10× objective (see ref. 13 for further details). For a given case, two or three tissue sections were photographed through each target areas. The images were first "flattened/skeletonized" to more readily distinguish objects of interest from background. A "threshold" overlay was then applied to each image to delineate the MBP fiber density. In the analysis of MBP immunostaining density, the "percentage of thresholded area" was determined for each image. Two cortical subregions were semiquantitatively analyzed. The first zone was centered in layer I (95 μm × 700 μm), and the second zone was aimed at layers II and III (215 μm × 700 μm). Three samples were obtained per section. As for the number of Olg+ cells, an area (1 mm × 1 mm) from the pial surface of the A1 with a ×20 objective was randomly chosen and then analyzed. Data were then recorded as an average value for each case. The experimenters performing the histological measurements reported in this study were blinded to the training status of the animals.

Electrophysiological Data Analysis. To generate cortical maps, Voronoi tessellation ("voronoi" is a Matlab function; Mathworks) was performed to create tessellated polygons, with the electrode penetration sites at their centers. Each polygon was assigned the characteristics (e.g., CF) of the corresponding penetration site (14). The boundaries of the primary auditory cortex were functionally determined using published criteria (14). The normalized tonotopic axis of CF maps was calculated by rotating the map to make horizontal a linear function fit of the penetration coordinates by using a least-squares method. The tonotopic index was assayed by computing the average minimum distance from each data point to the line connecting (0, 0) and (1, 1) after converting the logarithmic frequency range (1–30 kHz) to a linear range (0–1). RF overlap index was computed by first transforming the frequency–intensity response functions of two compared neurons into one-dimensional vectors and then calculating the peak of the normalized CC between the two vectors produced (15). These values were obtained for all permutations of neuron pairs with various interneuron distance recorded within a single A1 map.

RRTF and $F_{h1/2}$ data were quantified by determining the number of spikes that arrived within a fixed window (4–45 ms) after tone onset. Asynchronous responses were defined as the average spike rate encountered in a window starting at 45 ms after a noise burst to the time of occurrence of the next burst.

Misclassification rates were calculated using a published spike train distance metric (16) quantifying the similarity between two spike trains. First, the spike times were converted to spike trains using a resolution of 10 ms. Next, each spike train was convolved with an exponential function, $N(t) = N_0e^{-t/}t$, to obtain a filtered function. The distance between two spike trains was defined as the integral of the squared difference of the two functions. Distances were computed for all spike trains at different values of t. For analysis, we used a t of 10 ms as it empirically gave the best discriminability. A distance value was computed for every combination of spike trains obtained for the RRTF data for each recorded neuron. We then constructed confusion matrices by first calculating the average distance and SD between spike trains in response to the same or different pulsed noise stimuli presented at various repetition rates. For spike trains obtained with different stimuli, a misclassification occurred when the distance between the two trains was less than 1 SD away from the average distance (i.e., false negative); for spike trains recorded with identical stimuli, a misclassification occurred when the distance between the two trains was more than 1 SD away from the average distance (i.e., false positive).

We used the reverse correlation method to derive the STRF, which is the average spectrotemporal stimulus envelope immediately preceding a spike (STA) (17). Positive (red) regions of the STA indicate that stimulus energy at that frequency and time tended to increase the neuron's firing rate, and negative (blue) regions indicate where the stimulus envelope induced a decrease in firing rate (Fig. S3). For analysis related to STRFs, only neurons with CFs well within the sound range of the stimulus were used. CF distributions of neurons recorded were similar in the four groups (Fig. S3). To enable comparisons between neurons, each STRF was normalized to the absolute value of peak activation of the STA. Total activation and inhibition strength was then calculated as the integral of the positive or negative area of the STA more than 2 SDs away from the baseline.

We recorded spontaneous neuronal spikes simultaneously in silence from four electrodes to assess the degree of synchronization between cortical sites. CC functions were computed from each electrode pairs by counting the number of spikes with 1-ms bin size and were normalized by dividing each of its bins by the square root of the product of the number of discharges in both spike trains (18). The strength of the synchrony was then assessed by computing the average of the CC function from 10 ms preceding to 10 ms past the peak of the function. For neural synchrony recording, offline spike sorting using TDT OpenSorter (Tucker-Davis) was performed to include only single units in the analysis.

Normalized responses to standard and oddball tones were obtained by dividing the average firing rate recorded in the 50 ms after the occurrence of each tone presentation against the average firing rate observed during the 50 ms after the first standard or oddball tone in the sequence. Asymptotes and time constants ($\tau_{1/2}$) for standard and oddball responses were calculated by fitting exponential functions a least-squares method to the normalized response data for each recorded neuron. The method used to quantify probability coding in A1 has been previously described in detail (19, 20).

1. van Rossum MC (2001) A novel spike distance. *Neural Comput* 13:751–763.
2. deCharms RC, Blake DT, Merzenich MM (1998) Optimizing sound features for cortical neurons. *Science* 280:1439–1443.
3. Steen RG, Gronemeyer SA, Taylor JS (1995) Age-related changes in proton T1 values of normal human brain. *J Magn Reson Imaging* 5:43–48.
4. Peters A (2002) The effects of normal aging on myelin and nerve fibers: A review. *J Neurocytol* 31:581–593.
5. Ιtoyama Y, et al. (1980) Immunocytochemical method to identify myelin basic protein in oligodendroglia and myelin sheaths of the human nervous system. *Ann Neurol* 7:157–166.
6. Krukowski AE, Miller KD (2001) Thalamocortical NMDA conductances and intracortical inhibition can explain cortical temporal tuning. *Nat Neurosci* 4:424–430.
7. Elhilali M, Fritz JB, Klein DJ, Simon JZ, Shamma SA (2004) Dynamics of precise spike timing in primary auditory cortex. *J Neurosci* 24:1159–1172.
8. Blake DT, Merzenich MM (2002) Changes of AI receptive fields with sound density. *J Neurophysiol* 88:3409–3420.
9. Yazaki-Sugiyama Y, Kang S, Câteau H, Fukai T, Hensch TK (2009) Bidirectional plasticity in fast-spiking GABA circuits by visual experience. *Nature* 462:218–221.
10. Nelson SB, Turrigiano GG (2008) Strength through diversity. *Neuron* 60:477–482.
11. Contreras D, Palmer L (2003) Response to contrast of electrophysiologically defined cell classes in primary visual cortex. *J Neurosci* 23:6936–6945.
12. Blake DT, Merzenich MM (2002) Changes of AI receptive fields with sound density. *J Neurophysiol* 88:3409–3420.
13. Maciag D, et al. (2006) Neonatal antidepressant exposure has lasting effects on behavior and serotonin circuitry. *Neuropsychopharmacology* 31:47–57.
14. Bao S, Chang EF, Davis JD, Gobeske KT, Merzenich MM (2003) Progressive degradation and subsequent refinement of acoustic representations in the adult auditory cortex. *J Neurosci* 23:10765–10775.
15. Blake DT, et al. (2002) Sensory representation abnormalities that parallel focal hand dystonia in a primate model. *Somatosens Mot Res* 19:347–357.
16. van Rossum MC (2001) A novel spike distance. *Neural Comput* 13:751–763.

17. Escabi MA, Schreiner CE (2002) Nonlinear spectrotemporal sound analysis by neurons in the auditory midbrain. *J Neurosci* 22:4114–4131.
18. Brosch M, Schreiner CE (1999) Correlations between neural discharges are related to receptive field properties in cat primary auditory cortex. *Eur J Neurosci* 11:3517–3530.
19. Ulanovsky N, Las L, Nelken I (2003) Processing of low-probability sounds by cortical neurons. *Nat Neurosci* 6:391–398.
20. Ulanovsky N, Las L, Farkas D, Nelken I (2004) Multiple time scales of adaptation in auditory cortex neurons. *J Neurosci* 24:10440–10453.

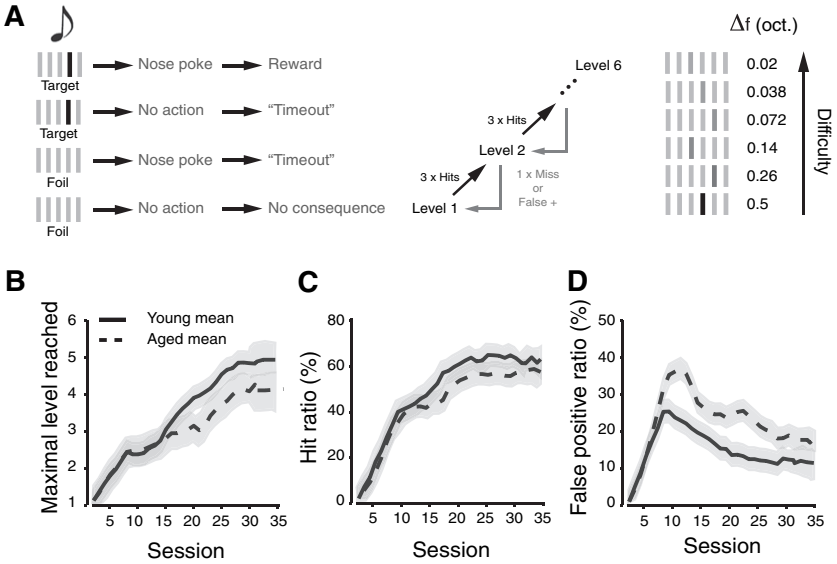

Fig. S1. Oddball discrimination training in young and aged rats. The performance of Y (n = 5) and A (n = 5) rats was determined in an oddball detection task. In this go/no-go experimental paradigm, rats were rewarded for performing a behavioral response only when an oddball tone was presented in a series of six otherwise identical tones. The difficulty level was increased by progressively reducing the frequency difference (Δf) between oddballs and standards after three consecutive hits were obtained. Lack of response to a target (miss) or a response to a series of six identical tones (false positive) resulted in a time-out and a decrease in the level of difficulty (staircase procedure, three-up/one-down). (*A*) Average maximal level reached by Y (solid line) and A (dotted line) adult rats as a function of training session number. (*B*) Average number of responses to targets over the total number of targets (hit ratio) in young and aged as a function of training session number. (*C*) Average number of responses to nontargets over the total number of nontargets (false-positive rate) as a function of training session number. Error bar represents SEM.

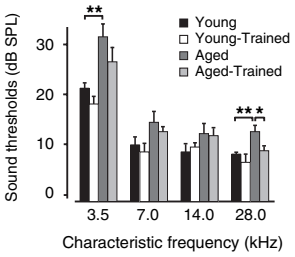

Fig. S2. Age-related changes in A1 sound intensity thresholds. Distribution of A1 sound intensity thresholds in Y, YT, A, and AT separated by CF. (Y, n = 14, number of sites, 387; YT, n = 5, number of sites, 211; A, n = 12, number of sites, 291, AT, n = 5, number of sites, 201.) Values shown are mean ± SEM. $^*P < 0.05$ and $^{**}P < 0.01$, t test with Bonferroni correction.

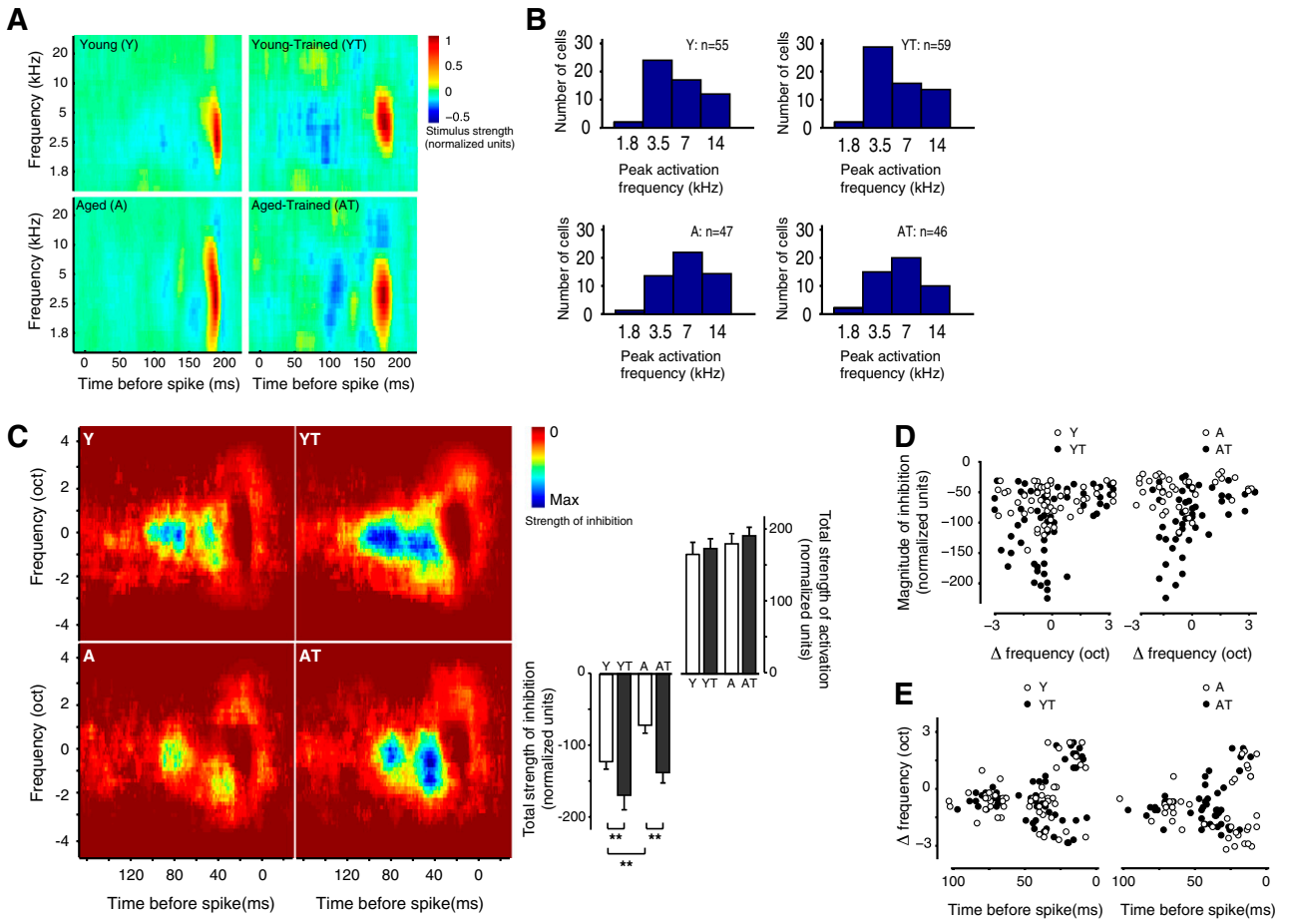

Fig. S3. Impact of training on spectrotemporal interactions. (*A*) Representative STRFs obtained for single neurons in A1 in all four experimental groups. Note the smaller and shallower inhibitory areas (blue) in the A group. (*B*) Distribution of neuron CFs of the neurons from which STRFs were obtained. (*C*) *Left*: Average normalized STRFs (inhibitory portion only) of all neurons recorded in each experimental group (*SI Methods*). Note the smaller and shallower inhibitory area (blue) in the A group and its recovery with training. The peak activation of each individual STRF was aligned to compute the average. (*C*) *Right*: Total average strengths in activation and inhibition of the STRFs recorded. (*D*) Intensity of inhibition and spectral distribution of the main inhibitory peak relative to the main peak of activation in all of the STRFs recorded in each group. (*E*) Temporal and spectral location of the main inhibitory peaks in all STRFs recorded. (Y, number of STRFs, 55; YT, number of STRFs, 59; A, number of STRFs, 47, AT, number of STRFs, 46.) Error bars represent SEM. $^{**}P < 0.001$, *t* test.

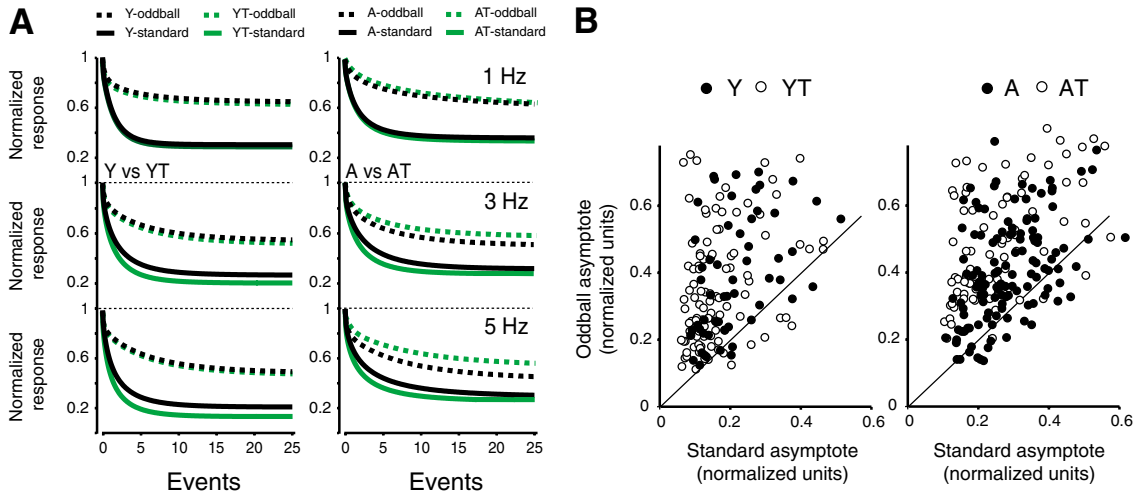

Fig. S4. Distractor suppression and novel stimulus discrimination in the aging A1. (*A*) Average exponential fit for responses to oddballs (dotted lines) and standards (full lines) in Y, YT, A, and AT at various rates of presentation. (*B*) Distribution of oddball to standard asymptote ratios for all neurons recorded in all four experimental groups. Note that the ratio is closer to 1 and increases with training in both trained groups. Y, number of neurons studied, 180; YT, number of neurons studied, 56; A, number of neurons studied, 216, AT, number of neurons studied, 167. Error bars represent SEM. $^{*}P < 0.05$.

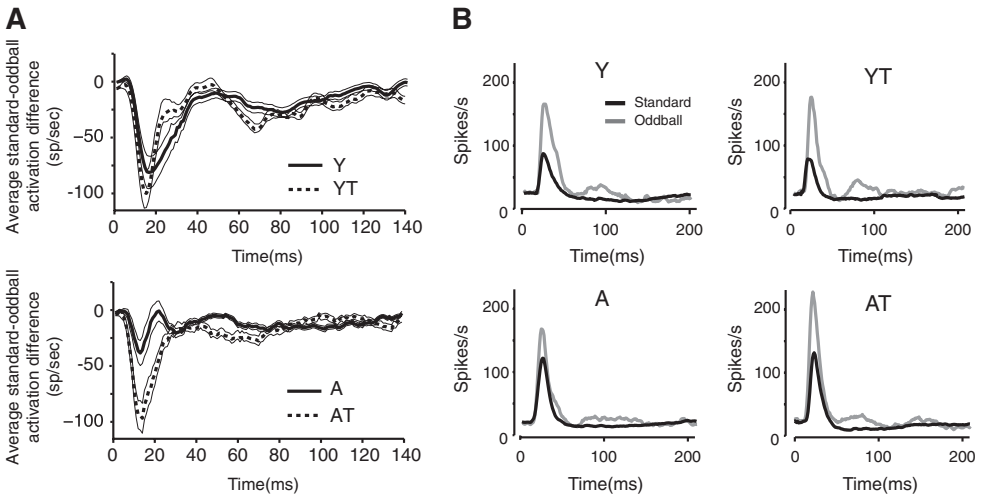

Fig. S5. Differences in cortical responses to low-probability stimuli. (*A*) Average difference between responses for standard and oddball tones ("oddball response salience", ORS) in both naive (full lines) and trained groups (dotted lines). Note the small ORS in the A group and how it recovers with training. (*B*), Average peristimulus time histogram (PSTH) for oddball and standard tones in all groups (all recorded neurons pooled). Recovery of ORS in AT is driven primarily by an increase in responses to oddball rather than a normalization of standard suppression. (Y, number of neurons, 180; YT, number of neurons, 56; A, number of neurons, 216; AT, number of neurons, 167.)

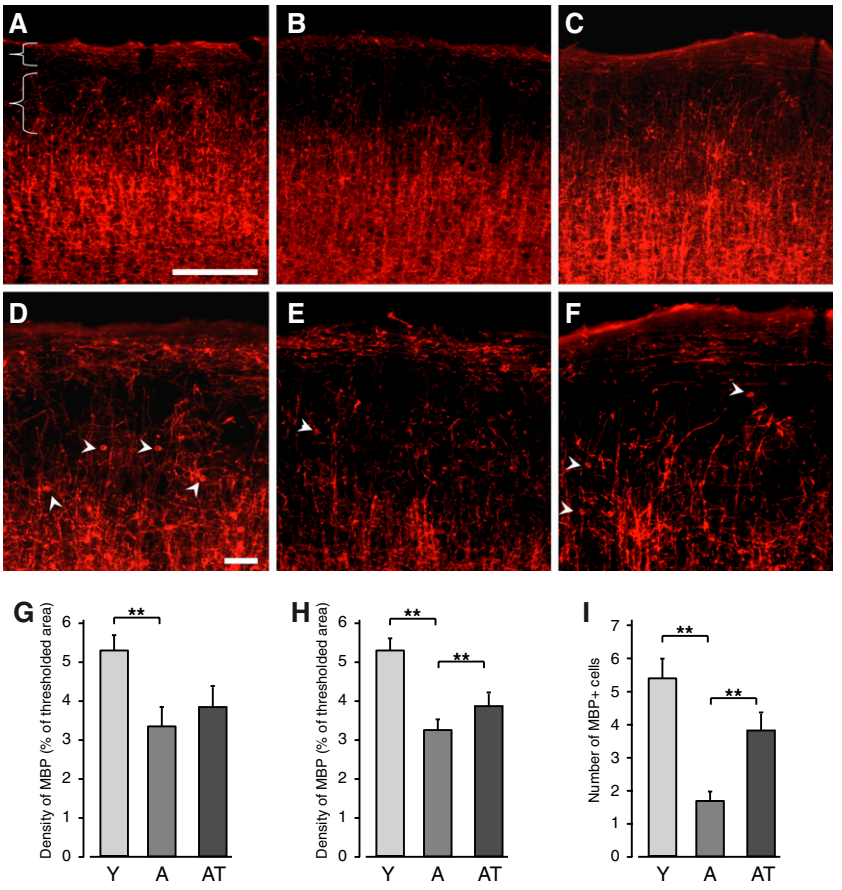

Fig. S6. Training-induced changes in cortical MBP expression in the aging cortex. Representative low and high powers of MBP immunoreactivity of A1 in Y (*A* and *D*), A (*B* and *E*), and AT (*C* and *F*) rats. Note the relative decrease in MBP staining in the superficial cortical layers (I–III) in the A group compared with the Y and YT groups. The semiquantitative analysis of MBP expression among the three experimental groups is shown in *G* (layer I), *H* (layer II and III), and *I* (number of Olg+ cells). The brackets marked the cortical layers I, and II, III, respectively, for the semiquantitative density analysis. [Scale bars: 300 μm in *A* (apply to *B* and *C*) and 100 μm in *D* (apply to *E* and *F*).] Number of hemispheres examined: Y, 6; A, 6; and AT, 6.